Bent by baryons: the low-mass galaxy-halo relation

Till Sawala,[1]* Carlos S. Frenk,[1] Azadeh Fattahi,[2] Julio F. Navarro,[2]
Richard G. Bower,[1] Robert A. Crain,[3,4] Claudio Dalla Vecchia,[5] Michelle Furlong,[1]
Adrian Jenkins,[1] Ian G. McCarthy,[4] Yan Qu,[1] Matthieu Schaller,[1] Joop Schaye[3]
and Tom Theuns[1]

[1]*Institute for Computational Cosmology, Department of Physics, University of Durham, South Road, Durham DH13LE, UK*
[2]*Department of Physics and Astronomy, University of Victoria, 3800 Finnerty Road, Victoria, BC V8P 5C2, Canada*
[3]*Leiden Observatory, Leiden University, Postbus 9513, NL-2300 RA Leiden, the Netherlands*
[4]*Astrophysics Research Institute, Liverpool John Moores University, 146 Brownlow Hill, Liverpool L3 5RF, UK*
[5]*Instituto de Astrofísica de Canarias, C/ Vía Láctea s/n, E-38205 La Laguna, Tenerife, Spain*

ABSTRACT

The relation between galaxies and dark matter haloes is of vital importance for evaluating theoretical predictions of structure formation and galaxy formation physics. We use hydrodynamic cosmological simulations of the Local Group to show that the widely used method of abundance matching based on dark matter only simulations fails at the low-mass end because two of its underlying assumptions are broken: only a small fraction of low-mass ($<10^{9.5}\,\mathrm{M_\odot}$) haloes host a visible galaxy, and baryon effects lower their growth rate. In this regime, reliance on dark matter only simulations for abundance matching is inappropriate and can lead to incorrect results. We find that the reported discrepancy between observational estimates of the halo masses of dwarf galaxies and the values predicted by abundance matching does not point to a failure of Λ cold dark matter, but simply to a failure to account for baryonic effects. Our results also imply that the Local Group contains only a few hundred observable galaxies in contrast with the thousands of faint dwarfs that abundance matching would suggest. We show how relations derived from abundance matching can be corrected, so that they can be used self-consistently to calibrate models of galaxy formation.

Key words: galaxies: abundances – galaxies: dwarf – galaxies: evolution – galaxies: formation – cosmology: theory.

1 INTRODUCTION

In the Λ cold dark matter (ΛCDM) paradigm (e.g. Davis et al. 1985; Frenk et al. 1988), stars form as gas cools in collapsed dark matter haloes (e.g. White & Rees 1978; White & Frenk 1991). The formation of galaxies involves both baryons and dark matter, but while only gas and stars are directly observable, numerical simulations of structure formation have largely been limited to the dark matter component, under the assumption that gravity is the only relevant force on large scales.

A conceptually simple and yet very powerful method to connect galaxies and haloes in this scenario, which does not require any detailed knowledge of the complex physics of galaxy formation, is abundance matching (e.g. Frenk et al. 1988; Yang, Mo & van den Bosch 2003; Kravtsov et al. 2004; Vale & Ostriker 2006; Guo et al. 2010; Moster et al. 2010; Behroozi, Wechsler & Conroy 2013;

Moster, Naab & White 2013). Assuming that a monotonic relation exists between some observable property of a galaxy (such as stellar mass) and some property of its dark matter halo (such as total mass), the relationship between both quantities can be computed from:

$$\int_{a_{h,min}}^{a_{h,max}} N_h(a_h)\mathrm{d}a_h = \int_{a_{\star,min}}^{a_{\star,max}} N_\star(a_\star)\mathrm{d}a_\star, \qquad (1)$$

where $N_h(a_h)$ and $N_\star(a_\star)$ are the numbers of haloes and galaxies in the same volume, with properties a_h and $a_\star$, whose maxima determine the upper limits $a_{h,max}$ and $a_{\star,max}$. For any lower limit, $a_{h,min}$, a corresponding lower limit, $a_{\star,min}$, is chosen such that equation (1) is satisfied, and the average relation $a_\star(a_h)$ is then uniquely determined.

Abundance matching is employed widely to infer quantities such as the stellar-to-total mass relation (e.g. Frenk et al. 1988; Yang et al. 2003; Guo et al. 2010; Moster et al. 2013). It has also been used to constrain the mass of the Milky Way's halo from its stellar mass (Guo et al. 2010), and to predict the total number of dwarf galaxies

* E-mail: till.sawala@durham.ac.uk

in the Local Group from an *N*-body simulation (Garrison-Kimmel et al. 2014).

Generally regarded as assumption-free, abundance matching results are often interpreted as direct predictions of the underlying cosmological model. They have also been used as a benchmark for models of galaxy formation physics, such as semi-analytic models (e.g. Guo 2011), and to calibrate hydrodynamic simulations (e.g. Scannapieco 2012; Munshi et al. 2013). However, models that reproduce the abundance matching relation for low-mass galaxies often require very strong feedback, which can result in an unrealistically high passive fraction (Fontanot et al. 2009; Weinmann et al. 2012; Moster et al. 2013). Conversely, many hydrodynamical simulations that produce realistic dwarf galaxies appear to have halo masses significantly below those inferred by abundance matching (e.g. Avila-Reese et al. 2011; Sawala et al. 2011).

In some cases, the stellar-to-total mass relation derived from abundance matching can also be compared directly to observations of individual galaxies. While they agree for galaxies in haloes more massive than $\sim 10^{12}\,M_\odot$ (Guo et al. 2010), discrepancies have been reported for lower mass haloes (Ferrero et al. 2012). In particular, dynamical mass estimates derived from stellar kinematics suggest stellar-to-total mass ratios for individual dwarf galaxies which are an order of magnitude higher than those inferred from abundance matching in ΛCDM.

Recently, we have shown that simulations that model the evolution of dark matter and baryons as a single fluid subject only to gravity (henceforth referred to as 'Dark Matter Only' or DMO simulations) do not produce the same abundance of haloes as hydrodynamic simulations that include the full baryonic effects. In particular, the collapse and subsequent expulsion of baryons by feedback processes reduce the mass of individual haloes (Sawala et al. 2013), a result that has since been reproduced and extended to higher masses (Cui, Borgani & Murante 2014; Velliscig et al. 2014).

Here, we use a new set of high-resolution hydrodynamical simulations of Local Group volumes to explore how the results of abundance matching are affected when the effects of baryons and the appearance of dark haloes are included self-consistently. Unlike models that are calibrated to reproduce an abundance matching relation based on a DMO simulation *before* baryons are taken into account, the stellar-to-total mass relation produced in our simulations is consistent with the relation we derive from abundance matching *after* the effects of baryons are included. Furthermore, this relation agrees with the dwarf galaxy data, thus demonstrating that the reported high stellar-to-total mass ratios of these galaxies are entirely consistent with the ΛCDM model.

This paper is organized as follows. In Section 2, we describe the simulations on which our work is based. In Section 3, we describe our results: the fraction of haloes that host galaxies is discussed in Section 3.1, the application to abundance matching in Section 3.2 and the implications in Section 3.3. We conclude with a summary in Section 4.

2 METHODS

We use a suite of cosmological 'zoom' simulations that each contain a pair of galaxies in haloes of $\sim 10^{12}\,M_\odot$ in a Local Group environment (see Fig. 1). In particular, we require that each volume contain two haloes of 5×10^{11}–$2.5 \times 10^{12}\,M_\odot$ separated by 800 ± 200 kpc, approaching with radial velocity of 0–250 km s^{-1} and with tangential velocity below 100 km s^{-1} in an environment with an unperturbed Hubble flow out to 4 Mpc. A total of 12 volumes were selected from the Dove simulation, a 100^3 Mpc^3 *N*-body simulation based on the *WMAP*-7 cosmology. The cosmological parameters and the linear phases of Dove, which are taken from the public multiscale Gaussian white noise field Panphasia, are given in tables 1 and 6 of Jenkins (2013), which also describes the method used to make the Local Group zoom initial conditions. The high-resolution initial
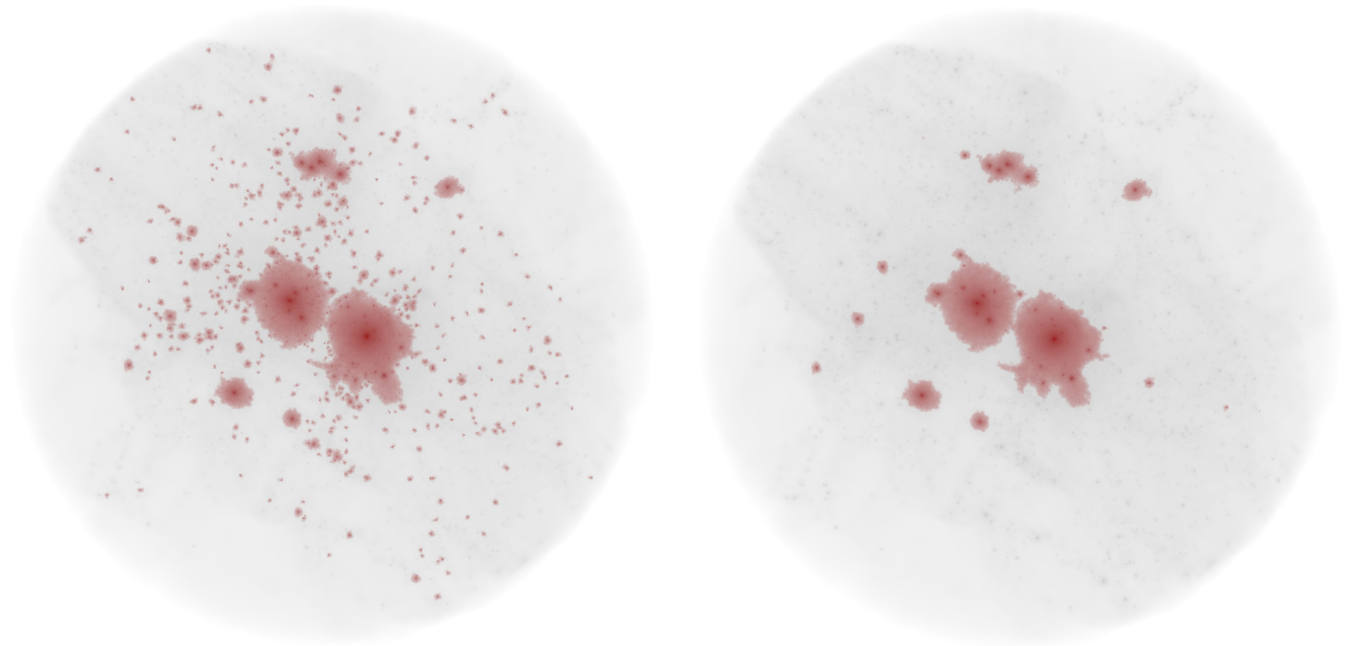

Figure 1. Projected density distribution of dark matter within 2 Mpc around the simulated Milky Way – M31 barycentre at $z = 0$ from one of our simulation volumes. Highlighted in red on top of the total mass distribution are particles in haloes above $5 \times 10^7\,M_\odot$ (left-hand panel), and particles in just those haloes that contain stars (right-hand panel).

Table 1. Numerical parameters of the simulations.

Label	Type	Particle masses		Max softening (pc/h)
		DM ($M_\odot$)	Gas ($M_\odot$)	
L1	Hydro	5.0×10^4	1.0×10^4	94
L1	DMO	6.0×10^4	–	94
L2	Hydro	5.9×10^5	1.3×10^5	216
L2	DMO	7.2×10^5	–	216
L3	Hydro	7.3×10^6	1.5×10^6	500
L3	DMO	8.8×10^6	–	500

conditions were set up using second-order Lagrangian perturbation theory as described in Jenkins (2010).

The simulations were performed using a pressure-entropy variant (Hopkins 2013) of the Tree-PM SPH code P-GADGET3 (Springel 2005), described in Dalla Vecchia et al. (in preparation). The subgrid physics model is an improved version of the model used in the Over-Whelmingly Large Simulations project (OWLS; Schaye 2010), that has been developed for the Evolution and Assembly of GaLaxies and their Environments project (EAGLE; Schaye 2015). In brief, the galaxy formation physics model includes metal-dependent radiative cooling (Wiersma, Schaye & Smith 2009a) and photoheating in the presence of a UV and X-ray background, and the cosmic microwave background (CMB). Prior to reionization, net cooling rates are computed from the CMB and from a UV and X-ray background that follows the $z = 9$ model of Haardt & Madau (2001) with a 1 Ryd high-energy cutoff. To mimic the temperature boost due to radiative transfer and non-equilibrium effects over the optically thin limit assumed in our simulations (Abel & Haehnelt 1999), we inject 2 eV per hydrogen and helium atom. We assume that hydrogen reionizes instantaneously at $z = 11.5$ (Planck XVI 2014), while the redshift dependence of helium reionization is modelled as a Gaussian centred at $z = 3.5$ (Theuns et al. 2002) with $\sigma(z) = 0.5$. As shown by Rollinde et al. (2013), the resultant evolution of the temperature–density relation is consistent with measurements of the intergalactic medium (Schaye et al. 2000).

Star formation follows Schaye & Dalla Vecchia (2008) with a metallicity-dependent threshold (Schaye 2004). The model includes stellar evolution (Wiersma et al. 2009b) and stochastic thermal supernova feedback (Dalla Vecchia & Schaye 2012), as well as black hole growth and AGN feedback (Springel, Di Matteo & Hernquist 2005; Booth & Schaye 2009; Rosas-Guevara 2013).

All simulations were run twice: once with gas and the baryon physics described above, and once as DMO. To investigate the regime of Local Group dwarf galaxies with stellar masses below $10^8 M_\odot$ and to demonstrate convergence, we use three different resolutions levels labelled L1, L2 and L3, whose parameters are given in Table 1. In the DMO simulations, the dark matter particle masses are larger by a factor of $(\Omega_b + \Omega_{DM})/\Omega_{DM}$ relative to the corresponding hydrodynamic simulations. For this work 12 volumes are analysed at L3, 5 volumes at L2 and 1 volume at L1. In addition, we have also rerun 1 volume at L3 and L2 without reionization.

We use a Friends-of-Friends algorithm (FoF, e.g. Davis et al. 1985) to identify overdense structures (FoF-groups), and the SUBFIND algorithm (Springel et al. 2001; Dolag et al. 2009) to identify self-bound substructures within them. As they represent the objects most directly associated with individual galaxies, we always refer to the self-bound substructures as 'haloes'. For central and isolated galaxies, the terms are largely synonymous, but satellite galaxies may share the same FoF-group while still residing in separate self-bound haloes.

3 RESULTS

3.1 The relevant abundance of haloes

The ejection of baryons from low-mass haloes through heating by the UV background (Okamoto, Gao & Theuns 2008) and supernova feedback reduces the growth rate of a halo and, as a result, its mass in the hydrodynamic simulation is lower than that of the corresponding object in the DMO simulation. Confirming results of our previous work (Sawala et al. 2013) based on the GIMIC simulations (Crain 2009), we find that the average mass of low-mass haloes is reduced by up to ~ 33 per cent relative to their counterparts in the DMO simulation. The universality of this behaviour at the low-mass end, also reproduced by Munshi et al. (2013), Khandai et al. (2014), Velliscig et al. (2014), indicates that it reflects a generic effect of feedback processes and baryon physics, only weakly dependent on the particular choice and parameters of the galaxy formation model.

In the simulations with reionization, we also find that a large fraction of haloes below $10^{9.5} M_\odot$ fail to form any stars. Photoionization has long been recognized as a possible mechanism to suppress star formation in low-mass haloes, through a reduction of cooling (e.g. Efstathiou 1992; Wiersma et al. 2009a) and through the heating and ejection of the interstellar medium (e.g. Okamoto et al. 2008; Pawlik & Schaye 2009). It can be an important factor in establishing the number of observable dwarf galaxies in the local universe (e.g. Kauffmann, White & Guiderdoni 1993; Bullock, Kravtsov & Weinberg 2000; Benson et al. 2002; Somerville 2002; Koposov et al. 2009; Okamoto & Frenk 2009).

In Fig. 1, we show the total dark matter distribution within 2 Mpc from the Local Group barycentre in one of our simulations. It can be seen that the majority of haloes above $5 \times 10^7 M_\odot$, which are highlighted in the left-hand panel, do not contain any stars, as highlighted in the right-hand panel. In Fig. 2, we compare the cumulative halo mass functions (left-hand column) and halo maximum circular velocity (v_{max}, the circular velocity measured at the radius where $v_{circ} = \sqrt{GM(<r)/r}$ is maximal) functions (right-hand column) obtained in the DMO and hydrodynamic simulations at $z = 0$. For the latter, we further distinguish between the total population of haloes, and the population of haloes that contain galaxies. The bottom panels show the ratios between the cumulative mass- and velocity-functions of the hydrodynamic and DMO simulations.

In all panels different shades indicate the resolution dependence: light lines correspond to L3, intermediate to L2 and dark to L1, the highest resolution simulation. The apparent fraction of dark haloes still decreases between L3 and L2, where the minimum stellar mass decreases by a factor of 12, from $\sim 1.5 \times 10^6 M_\odot$ to $\sim 1.3 \times 10^5 M_\odot$. However, a further decrease of this minimum stellar mass by the same factor to $\sim 10^4 M_\odot$ at L1 only has a very small effect on the total number of galaxies in haloes above $10^8 M_\odot$, and the corresponding dark fraction. The number of 'galaxies', i.e. the fraction of haloes in which any stars have formed, has thus converged at L2.

In the hydrodynamic simulations, the reduced growth rate of haloes below $\sim 10^{10} M_\odot$, or v_{max} below ~ 70 km s^{-1}, results in lower masses and a reduced halo abundance. More importantly, confirming earlier results by e.g. Crain et al. (2007), Okamoto et al. (2008), Okamoto & Frenk (2009) and Pawlik & Schaye (2009), we find that reionization prevents star formation in most haloes below $\sim 10^{9.5} M_\odot$ ($v_{max} \sim 25$ km s^{-1}). We find a continuous decline in the galaxy fraction, from ~ 100 per cent of all haloes at $5 \times 10^9 M_\odot$ to <5 per cent at $10^8 M_\odot$. Reflecting the fact that the probability of star formation strongly depends on a halo's formation history and
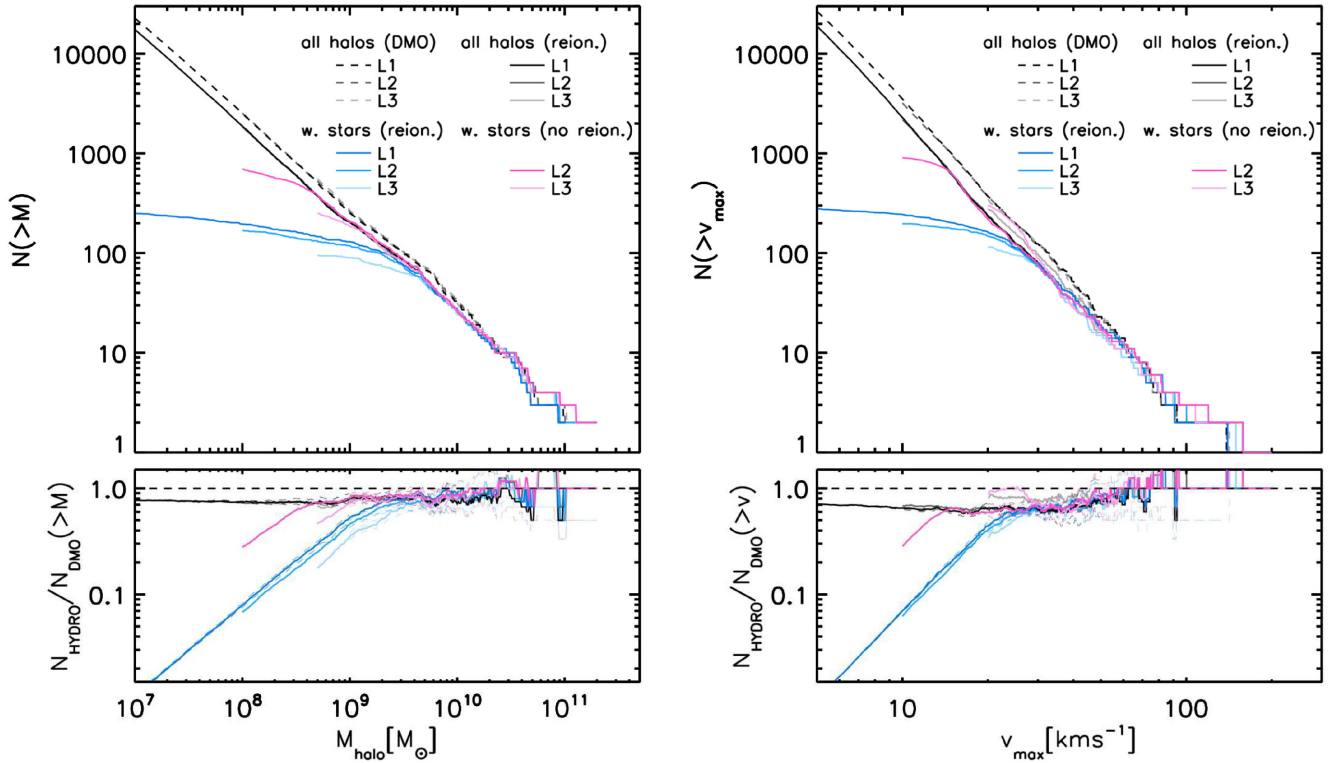
Figure 2. Top: cumulative halo mass function (left) and maximum circular velocity function (right) in one of our simulated LG volumes, in DMO simulations (dashed lines) and in hydrodynamic simulations (solid lines) at $z = 0$. Grey lines show the results counting all haloes, while coloured lines count only haloes that contain at least one star particle; blue for the simulation with reionization and purple for the simulation without reionization. In each case, lightly coloured lines are obtained from L3, medium colours from L2 and dark colours from L1. Bottom: ratio of the cumulative halo mass function (left) and maximum circular velocity function (right), relative to the DMO results. Dashed lines also indicate the 1σ scatter, from all 12 volumes at L3 for $M > 10^{10}\,\mathrm{M_\odot}$, $v_\mathrm{max} > 50\,\mathrm{km\,s^{-1}}$, 5 volumes at L2 for $10^9 < M < 10^{10}\,\mathrm{M_\odot}$, $30 < v_\mathrm{max} < 50\,\mathrm{km\,s^{-1}}$; and 1 volume at L1 for $M < 10^9\,\mathrm{M_\odot}$, $v_\mathrm{max} < 20\,\mathrm{km\,s^{-1}}$. While the fraction of dark haloes decreases significantly from L3 to L2 where the threshold stellar mass decreases from $5 \times 10^6\,\mathrm{M_\odot}$ to $4.2 \times 10^5\,\mathrm{M_\odot}$, the results are converged for L2 in the simulations that include reionization.

binding energy, the resulting decline is steeper when expressed in terms of v_max.

In the simulations without reionization, dark haloes only appear for halo masses below $10^{8.5}\,\mathrm{M_\odot}$ or velocities below $12\,\mathrm{km\,s^{-1}}$ at L2. In this (unrealistic) scenario, the total number of galaxies is not converged in our simulations, and is likely to increase further with higher resolution. By contrast, the inclusion of reionization provides an upper limit to the number of galaxies that is independent of resolution at the level reached in our simulations.

It is also worth noting that while the abundance of objects in the hydrodynamical simulations with reionization is always at or below the DMO case in terms of halo mass, it can exceed the DMO case in terms of v_max for haloes with $v_\mathrm{max} > {\sim}100\,\mathrm{km\,s^{-1}}$. In these massive haloes, cooling is efficient, baryons are largely processed inside the halo and adiabatic contraction can lead to an increase of concentration and v_max, without changing the total halo mass. We note, however, that as a result of AGN feedback, the abundance of haloes is reduced up to much higher masses (Cui et al. 2014; Velliscig et al. 2014).

3.2 Abundance matching in the real universe

While the reduction in average halo mass due to baryons is noticeable, the steeply declining fraction of haloes that contain observable galaxies has the strongest impact on abundance matching for haloes below $3 \times 10^9\,\mathrm{M_\odot}$.

We stress that in order to relate observed galaxies to their dark matter haloes via abundance matching, only those haloes that host galaxies should be taken into account. Defining the total mass function, $N'_\mathrm{h}(m)$, as the mass function of all dark matter haloes irrespective of occupation, and the *reduced halo mass function*, $N_\mathrm{h}(m)$, as the mass function of haloes *that host galaxies*, we can derive the combined effects of the influence of baryons on halo mass, and the incomplete occupation of haloes by galaxies. Matching $N_\mathrm{h}(m)$ as measured in our hydrodynamic simulation to $N'_\mathrm{h}(m)$ as measured in the corresponding DMO simulation,

$$\int_{M_\mathrm{h}}^{M_\mathrm{h,max}} N_\mathrm{h}(m)\,\mathrm{d}m = \int_{M'_\mathrm{h}}^{M'_\mathrm{h,max}} N'_\mathrm{h}(m)\,\mathrm{d}m, \qquad (2)$$

we can compute the mass $M_\mathrm{h}(M'_\mathrm{h})$ of haloes containing galaxies in the hydrodynamic simulation for which the cumulative abundance equals that of all haloes of mass M'_h in the DMO simulation.

As shown in Fig. 3, for $M'_\mathrm{h} = 2 \times 10^9 - 10^{10}\,\mathrm{M_\odot}$, we find a good fit to the relation $M_\mathrm{h}(M'_\mathrm{h})$ by functions of the form

$$M_\mathrm{h}(M'_\mathrm{h}) = \frac{\alpha M'_\mathrm{h}}{1 + (M'_\mathrm{h}/M_0)^\beta}, \qquad (3)$$

where $0 < \alpha < 1$ and $\beta < -1$. The high-mass asymptote $M_\mathrm{h} = \alpha M'_\mathrm{h}$ results from the reduction in halo mass by baryon effects, while the low-mass asymptote $M_\mathrm{h} = \alpha M_0^\beta M'^{1-\beta}_\mathrm{h}$ is caused by the steep decline in the fraction of luminous haloes below M_0. When
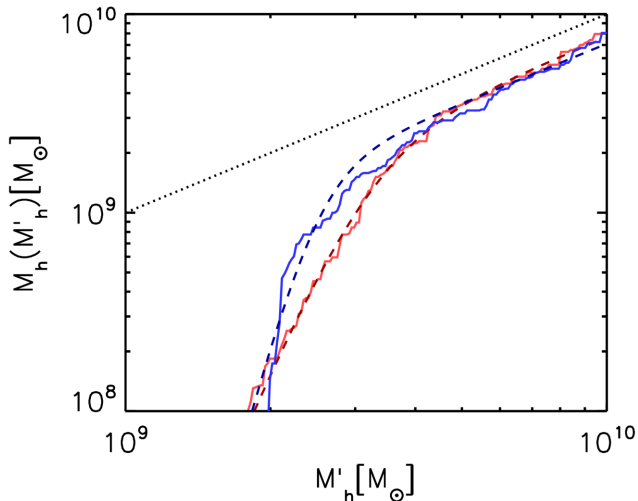
Figure 3. Mass of haloes containing galaxies in the hydrodynamic simulation, as a function of the halo mass in the DMO simulation corresponding to the same cumulative abundance. Solid curves indicate results at $z = 0$ (red) and at peak mass (blue), dashed curves show the respective fits of equation (3) over the plotted mass interval. For guidance, the dotted black line indicates a 1:1 relation, which corresponds to no baryon effects and all haloes populated by galaxies.

measured at $z = 0$, we find values of $\alpha = 0.76$, $M_0 = 3.2 \times 10^9 \, \mathrm{M_\odot}$ and $\beta = -4.7$.

For a galaxy of a given stellar mass, equation (3) maps the mass, M'_h, of the associated halo from a DMO simulation to a (lower) mass, M_h, taking into account the reduction in halo masses due to baryon effects, as well as the partial occupation of haloes by galaxies.

As abundance matching is commonly applied to the peak mass that a halo attains, rather than to the current mass (which can be reduced by tidal stripping after infall in the case of satellites), we repeat our analysis for the same set of haloes selected at $z = 0$, but using the peak mass for both M_h and M'_h. Here, we find values of $\alpha = 0.71$, $M_0 = 2.5 \times 10^9 \, \mathrm{M_\odot}$ and $\beta = -8$, but note that the luminous fraction among haloes with peak masses at $\sim 10^9 \, \mathrm{M_\odot}$ in our simulation is so low that the value of β is poorly constrained.

The relation $M_h(M'_h)$ allows us to obtain an expression for the stellar-to-total mass relation expected in a universe with baryons and both luminous and dark haloes, given a stellar-to-halo mass relation previously obtained from abundance matching, where a DMO simulation and a complete occupation of haloes by galaxies had been assumed:

$$\left.\frac{m_\star}{m_{\mathrm{H}}}\right|(M_{\mathrm{h}}) = \left.\frac{m_\star}{m_{\mathrm{H}}}\right|_{\mathrm{DMO}}(M'_{\mathrm{h}}), \tag{4}$$

under the assumption that there is no significant change in the correlation between average halo mass and galaxy mass.

Since those haloes that are predicted not to host any galaxy are excluded from the *reduced halo* mass function, galaxies are now assigned to haloes of lower masses than they would have been in the DMO simulation, increasing their stellar-to-total mass ratios. By analogy, if galaxies exist that do not belong to any dark matter haloes (e.g. 'tidal dwarf galaxies'), we would require a *reduced galaxy* stellar mass function, with the effect of decreasing the average stellar-to-total mass ratios. However, such objects are not found in our simulations.
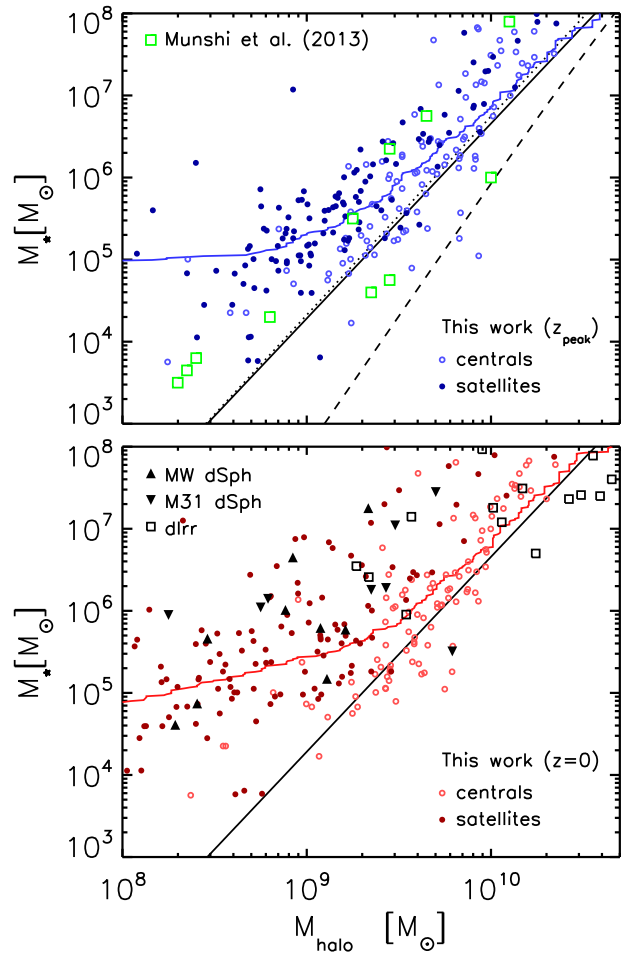

Figure 4. Stellar-to-total mass relation for galaxies as a function of peak halo mass (top) and of halo mass at $z = 0$ (bottom). The black lines show abundance matching results from DMO simulations by Guo et al. (2010, dashed), Wang & Jing (2010, dotted) and Moster et al. (2013, solid, reproduced in both the panels). The blue solid line (top) and red solid line (bottom) show the results of Moster et al. (2013) after our correction for the effect of baryons and dark haloes. In both the panels, circles show the results for central galaxies (open circles) and satellite galaxies (filled circles) as measured in our simulations. In the top panel, green squares denote results of hydrodynamic simulations by Munshi et al. (2013), which are tuned to reproduce the original abundance matching relation. In the bottom panel, we compare our results at $z = 0$ to observations of individual M31 and MW dwarf spheroidal galaxies (triangles, Peñarrubia, McConnachie & Navarro 2008; Woo, Courteau & Dekel 2008; Misgeld & Hilker 2011; Tollerud 2012), and dwarf irregular galaxies (squares, Côté, Carignan & Freeman 2000; McGaugh 2005; Stark, McGaugh & Swaters 2009; Oh et al. 2011; Ferrero et al. 2012).

In Fig. 4, we show the resulting change in the stellar-to-total mass relations, with halo masses measured at peak mass (top), or at $z = 0$ (bottom). The black lines show the results based on standard abundance matching of DMO simulations by Guo et al. (2010, dashed), Wang & Jing (2010, dotted) and Moster et al. (2013, solid), while the blue line (top panel) and red line (bottom panel) show the relation of Moster et al. (2013) after our correction for baryonic effects and the presence of dark haloes.

The newly derived stellar-to-total mass relations shown in Fig. 4 express the typical halo mass associated with a galaxy of a given stellar mass. It is important to note that where the occupation of

haloes by galaxies is incomplete, these relations are no longer equivalent to the relations that describe the stellar mass for a given halo mass. Indeed, in the mass range where most haloes are dark, the typical stellar mass of a halo is zero. This distinction is crucial where predictions from abundance matching are compared to either observations or simulations of individual galaxies.

In both panels, it can be seen that the typical stellar mass of galaxies in haloes of $10^9 \, \mathrm{M}_\odot$ is increased by an order of magnitude, and in haloes of $3 \times 10^8 \, \mathrm{M}_\odot$, it is increased by almost two orders of magnitude. This change in the stellar-to-total mass ratio can be greater than the differences between individual abundance matching models that are shown in the top panel and which account for differences in the stellar mass function, cosmology, assumed scatter and treatment of satellites. In other words, abundance matching applied to DMO simulations that do not account for baryons fail to constrain any of the other parameters in the dwarf galaxy regime.

It can also be seen from Fig. 4 that the faint end tail of the stellar-to-total mass relation deviates from the single power-law form which was originally introduced by Yang et al. (2003) and that is assumed in most abundance matching models.

3.3 Abundance matching, observations and hydrodynamic simulations

The stellar and total masses measured for galaxies and haloes in our simulation at L1 are indicated by circles in both the panels in Fig. 4. Both at $z = 0$ and at peak mass, these values agree well with the stellar-to-total mass relations derived from abundance matching when baryons are taken into account, as described in Section 3.2, but not with the original DMO abundance matching results.

The bottom panel of Fig. 4 also includes a comparison to observational data from Milky Way and M31 satellite galaxies, and dwarf irregular galaxies. For the MW satellites we use virial masses estimated by Peñarrubia et al. (2008), while for M31 satellites we convert $v_{\max}$ estimates by Tollerud (2012) using the relation for satellites given by Klypin, Trujillo-Gomez & Primack (2011). For the dwarf irregulars, we show m_{200} for the best-fitting NFW profile as measured by Ferrero et al. (2012), limiting the sample to galaxies where the velocity profile is measured to at least $r_{\mathrm{out}} = 200 \, \mathrm{pc}$.

For consistency with the observations, the halo masses at $z = 0$ of individual objects in the simulation are derived using the measured maximum circular velocity converted to mass following Klypin et al. (2011). While these observed mass estimates still involve a high degree of uncertainty, our simulation and the corrected abundance matching relation are both in good agreement with the observational data. The discrepancy between abundance matching and the measurements of individual galaxies reported by Ferrero et al. (2012) is resolved once the abundance of haloes is corrected.

It is worth remembering that abundance matching based on halo masses from DMO simulations generally also results in baryon fractions of dwarf galaxies far below the universal value. This already indicates a change in total halo mass, and exposes a limitation of using DMO simulations on these scales.

Also shown by green symbols in the top panel of Fig. 4 are the results of hydrodynamical simulations by Munshi et al. (2013), which 'successfully' reproduce the abundance matching relation obtained from a DMO simulation. Note here that at $2 \times 10^8 \, \mathrm{M}_\odot$, fewer than 1 in 10 haloes host a galaxy in our simulations, whereas the relation reproduce by Munshi et al. (2013) assumes all haloes to be populated. As the stellar-to-total mass ratios diverge at low masses from those obtained in our simulation (blue symbols), the assumed models of galaxy formation physics must differ. In par-

ticular, in order to satisfy the constraints imposed by abundance matching based on DMO simulations, Munshi et al. (2013) impose a very low star formation efficiency due to processes like supernova feedback. Our results suggest that a reliance on abundance matching based on DMO simulations can lead to artificial conclusions for both cosmology and astrophysics.

It is also worth noting that the overwhelming majority of 'dark' haloes in our simulations with reionization are not only devoid of star particles, but also free of gas that could potentially result in star formation. Based on these results, we predict that the Local Group only contains a few hundred dwarf galaxies within a radius of 2.5 Mpc. This is in contraction to recent results obtained from DMO simulations and abundance matching by Garrison-Kimmel et al. (2014) who predict thousands of as-yet undiscovered faint dwarf galaxies. Under the classical assumption of abundance matching that all haloes host galaxies, these authors assign higher halo masses to the observed galaxies, and predict a larger total number of galaxies for the same halo mass range. By contrast, we find that an increasingly sparse occupation of low-mass haloes by galaxies results in a greater halo mass range assigned to the same number of observed galaxies. We predict that the Local Group should contain thousands of dark matter haloes, only a small fraction of which contain galaxies.

4 SUMMARY

The commonly used method of abundance matching between *N*-body DMO simulations and the observed stellar mass function is not assumption free: it relies on the implicit assumption that structure formation can be represented by DMO simulations and that every halo hosts a galaxy. Using a set of high-resolution simulations of Local Group volumes with and without baryons, we have shown that, at the low-mass end, both of these assumptions are broken. Because of cosmic reionization, most haloes below $3 \times 10^9 \, \mathrm{M}_\odot$ do not contain an observable galaxy. In this regime, the median stellar-to-total mass relation inferred directly from abundance matching only applies to (mostly unobservable) haloes, but has no direct application to observable galaxies.

Our simulations assume reionization in the optically thin limit without self-shielding, and radiative cooling which does not include molecular cooling at low temperatures. While these limitations may influence the impact of reionization on star formation rates in existing galaxies, the proto-galaxies that are prevented from star formation in our simulations reach neither the gas densities required for self-shielding nor the metallicities required for molecular cooling after reionization. Of course, our simulations cannot resolve the formation of Pop-III stars from primordial gas. Our results also assume that reionization is uniform and local variations might change the impact for individual galaxies. A different time of reionization would also affect the fraction of haloes that can host galaxies. However, under the assumption that hydrogen reionization takes place at $z = 11.5$ (Planck XVI 2014), our simulations result in a fraction of dark haloes sufficient to reconcile previously reported tensions between CDM-based abundance matching and measurements of individual dwarf galaxies.

By equating the cumulative abundances of objects from hydrodynamical and DMO simulations, we have shown how abundance matching results can be modified to account for baryonic effects. We stress that a reliance on the results from abundance matching obtained through dark matter only simulations can have serious consequences: it can lead to erroneous conclusions about cosmology, and, when used as a benchmark for hydrodynamic simulations or

semi-analytical models, it can also lead to false conclusions about galaxy formation physics. Baryon effects have to be taken into account self-consistently for abundance matching to give a meaningful interpretation of the connection between galaxies and haloes.

REFERENCES

Abel T., Haehnelt M. G., 1999, ApJ, 520, L13
Avila-Reese V., Colín P., González-Samaniego A., Valenzuela O., Firmani C., Velázquez H., Ceverino D., 2011, ApJ, 736, 134
Behroozi P. S., Wechsler R. H., Conroy C., 2013, ApJ, 770, 57
Benson A. J., Frenk C. S., Lacey C. G., Baugh C. M., Cole S., 2002, MNRAS, 333, 177
Booth C. M., Schaye J., 2009, MNRAS, 398, 53
Bullock J. S., Kravtsov A. V., Weinberg D. H., 2000, ApJ, 539, 517
Côté S., Carignan C., Freeman K. C., 2000, AJ, 120, 3027
Crain R. A., Eke V. R., Frenk C. S., Jenkins A., McCarthy I. G., Navarro J. F., Pearce F. R., 2007, MNRAS, 377, 41
Crain R. A. et al., 2009, MNRAS, 399, 1773
Cui W., Borgani S., Murante G., 2014, MNRAS, 441, 1769
Dalla Vecchia C., Schaye J., 2012, MNRAS, 426, 140
Davis M., Efstathiou G., Frenk C. S., White S. D. M., 1985, ApJ, 292, 371
Dolag K., Borgani S., Murante G., Springel V., 2009, MNRAS, 399, 497
Efstathiou G., 1992, MNRAS, 256, 43p
Ferrero I., Abadi M. G., Navarro J. F., Sales L. V., Gurovich S., 2012, MNRAS, 425, 2817
Fontanot F., De Lucia G., Monaco P., Somerville R. S., Santini P., 2009, MNRAS, 397, 1776
Frenk C. S., White S. D. M., Davis M., Efstathiou G., 1988, ApJ, 327, 507
Garrison-Kimmel S., Boylan-Kolchin M., Bullock J. S., Lee K., 2014, MNRAS, 438, 2578
Guo Q., White S., Li C., Boylan-Kolchin M., 2010, MNRAS, 404, 1111
Guo Q. et al., 2011, MNRAS, 413, 101
Haardt F., Madau P., 2001, in Neumann D. M., Tran J. T. V., eds, Proc. XXXVIth Rencontres de Moriond, Clusters of Galaxies and the High Redshift Universe Observed in X-rays CEA, Paris
Hopkins P. F., 2013, MNRAS, 428, 2840

Jenkins A., 2010, MNRAS, 403, 1859
Jenkins A., 2013, MNRAS, 434, 2094
Kauffmann G., White S. D. M., Guiderdoni B., 1993, MNRAS, 264, 201
Khandai N., Di Matteo T., Croft R., Wilkins S. M., Feng Y., Tucker E., DeGraf C., Liu M.-S., 2014, preprint (arXiv:e-prints)
Klypin A. A., Trujillo-Gomez S., Primack J., 2011, ApJ, 740, 102
Koposov S. E., Yoo J., Rix H.-W., Weinberg D. H., Macciò A. V., Escudé J. M., 2009, ApJ, 696, 2179
Kravtsov A. V., Berlind A. A., Wechsler R. H., Klypin A. A., Gottlöber S., Allgood B., Primack J. R., 2004, ApJ, 609, 35
McGaugh S. S., 2005, ApJ, 632, 859
Misgeld I., Hilker M., 2011, MNRAS, 414, 3699
Moster B. P., Somerville R. S., Maulbetsch C., van den Bosch F. C., Macciò A. V., Naab T., Oser L., 2010, ApJ, 710, 903
Moster B. P., Naab T., White S. D. M., 2013, MNRAS, 428, 3121
Munshi F. et al., 2013, ApJ, 766, 56
Oh S.-H., de Blok W. J. G., Brinks E., Walter F., Kennicutt R. C., Jr, 2011, AJ, 141, 193
Okamoto T., Frenk C. S., 2009, MNRAS, 399, L174
Okamoto T., Gao L., Theuns T., 2008, MNRAS, 390, 920
Pawlik A. H., Schaye J., 2009, MNRAS, 396, L46
Peñarrubia J., McConnachie A. W., Navarro J. F., 2008, ApJ, 672, 904
Planck XVI 2014, A&A, 571, A16
Rollinde E., Theuns T., Schaye J., Pâris I., Petitjean P., 2013, MNRAS, 428, 540
Rosas-Guevara Y. M. et al., 2013, preprint (arXiv:1312.0598)
Sawala T., Guo Q., Scannapieco C., Jenkins A., White S., 2011, MNRAS, 413, 659
Sawala T., Frenk C. S., Crain R. A., Jenkins A., Schaye J., Theuns T., Zavala J., 2013, MNRAS, 431, 1366
Scannapieco C. et al., 2012, MNRAS, 423, 1726
Schaye J., 2004, ApJ, 609, 667
Schaye J., Dalla Vecchia C., 2008, MNRAS, 383, 1210
Schaye J., Theuns T., Rauch M., Efstathiou G., Sargent W. L. W., 2000, MNRAS, 318, 817
Schaye J. et al., 2010, MNRAS, 402, 1536
Schaye J. et al., 2015, MNRAS, 446, 521
Somerville R. S., 2002, ApJ, 572, L23
Springel V., 2005, MNRAS, 364, 1105
Springel V., White S. D. M., Tormen G., Kauffmann G., 2001, MNRAS, 328, 726
Springel V., Di Matteo T., Hernquist L., 2005, MNRAS, 361, 776
Stark D. V., McGaugh S. S., Swaters R. A., 2009, AJ, 138, 392
Theuns T., Schaye J., Zaroubi S., Kim T.-S., Tzanavaris P., Carswell B., 2002, ApJ, 567, L103
Tollerud E. J. et al., 2012, ApJ, 752, 45
Vale A., Ostriker J. P., 2006, MNRAS, 371, 1173
Velliscig M., van Daalen M. P., Schaye J., McCarthy I. G., Cacciato M., Le Brun A. M. C., Dalla Vecchia C., 2014, MNRAS, 442, 2641
Wang L., Jing Y. P., 2010, MNRAS, 402, 1796
Weinmann S. M., Pasquali A., Oppenheimer B. D., Finlator K., Mendel J. T., Crain R. A., Macciò A. V., 2012, MNRAS, 426, 2797
White S. D. M., Frenk C. S., 1991, ApJ, 379, 52
White S. D. M., Rees M. J., 1978, MNRAS, 183, 341
Wiersma R. P. C., Schaye J., Smith B. D., 2009a, MNRAS, 393, 99
Wiersma R. P. C., Schaye J., Theuns T., Dalla Vecchia C., Tornatore L., 2009b, MNRAS, 399, 574
Woo J., Courteau S., Dekel A., 2008, MNRAS, 390, 1453
Yang X., Mo H. J., van den Bosch F. C., 2003, MNRAS, 339, 1057

This paper has been typeset from a TEX/LATEX file prepared by the author.